Structure and Variability of the Jan Mayen Current in the Greenland Sea Gyre From a Yearlong Mooring Array

V. Pellichero[1] [ID]**, C. Lique[1]** [ID]**, N. Kolodziejczyk[1]** [ID]**, and K. Balem[1]** [ID]

[1]University of Brest, CNRS, IRD, Ifremer, Laboratoire d'Océanographie Physique et Spatiale (LOPS), IUEM, Brest, France

Abstract The Jan Mayen Channel is located North of the Jan Mayen Island in the Nordic Seas, and is an important gateway for the exchanges of volume, heat and freshwater between the Greenland and the Norwegian basins via the Jan Mayen Current. Based on observations from moored instruments deployed on the shelf and the continental slope of the Jan Mayen Island from August 2017 to August 2018, we document the mean state and the variability of the currents, temperature and salinity and their associated vertical structure. We found that the main feature of circulation is an intense and permanent south-eastward jet-like current centered at 150 m depth, located on the 400 m depth slope, with a maximum mean magnitude of 7 cm·s⁻¹. While the velocities recorded on the shelf are largely constant in speed and direction, without any strong seasonal cycle, the moorings located offshore are capturing larger anomalies on short time scales that are likely the signature of eddies passing across the mooring array. Overall, the variability of the transport across the section is correlated with the large-scale wind pattern over the Nordic Seas, highlighting that the Jan Mayen Current is part of a complex system of currents that operates at larger scale in the region.

Plain Language Summary Located at the junction of the ridges separating the Iceland, Greenland, and Norwegian basins, the Jan Mayen Channel is considered as a route for Greenland Sea water entering into the Norwegian Sea. In 2017–2018, a high-resolution (6 km spacing mean) mooring array was deployed at the entrance of the Jan Mayen Channel. This array consisting of six moorings progressing onshore to offshore provides a great opportunity to investigate water transport between Greenland and Norwegian Seas via the Jan Mayen Current. We reveal that the Jan Mayen Current presents different behaviors on the shelf and in the channel and we find that the current at the entrance of the channel is characterized by a strong jet-like structure attached on the shelf with an intensity of about 7 cm·s⁻¹. Thus, over 2017–2018, the Jan Mayen Channel was a regular and direct route for intermediate and deep water from the Greenland Sea to the Norwegian Sea.

1. Introduction

The Nordic Seas (i.e., the Greenland, Iceland, and Norwegian Seas) are the gateway for the exchanges between mid and high latitudes as they connect two major basins: the Arctic Ocean in the north and the Atlantic Ocean in the south. Hence, they play a central role in the global climate system as it is the main region where Atlantic origin waters are transformed into waters that are dense enough to feed the lower limb of the Atlantic Meridional Overturning Circulation. The local dynamics in each of these basins is very peculiar and controls in various ways the rate at which ocean tracers such as heat and carbon are transferred from the surface to the interior. The Norwegian Sea is largely responsible for the intense cooling of the Atlantic Water whereas the Greenland and Iceland Seas are mostly involved in intermediate and deep water formation (Isachsen et al., 2007; Petit et al., 2020; Swift & Aagaard, 1981).

In the Nordic Seas, the surface circulation is mostly cyclonic, with the eastern part dominated by the Norwegian Atlantic Current carrying Atlantic-origin warm and salty water northward, while the western part is dominated by the East Greenland Current (EGC) carrying Polar-origin cold and fresher water southward (Jakobsen et al., 2003; Figure 1).

Situated just North of the Jan Mayen Island, the Jan Mayen Channel (JMCh) is considered as a direct route for Greenland Sea water to enter the Norwegian Sea (Hansen & Østerhus, 2000; Swift & Koltermann, 1988). It is also the deepest passage between those two basins as it reaches 2,200 m (Østerhus & Gammelsrød, 1999). The Norwegian Sea Deep Water (NSDW), formed from a mixture of deep waters from the Greenland Sea (GSDW) and the Arctic Ocean, enters the Norwegian basin through a complex multi-passage outflow system, which
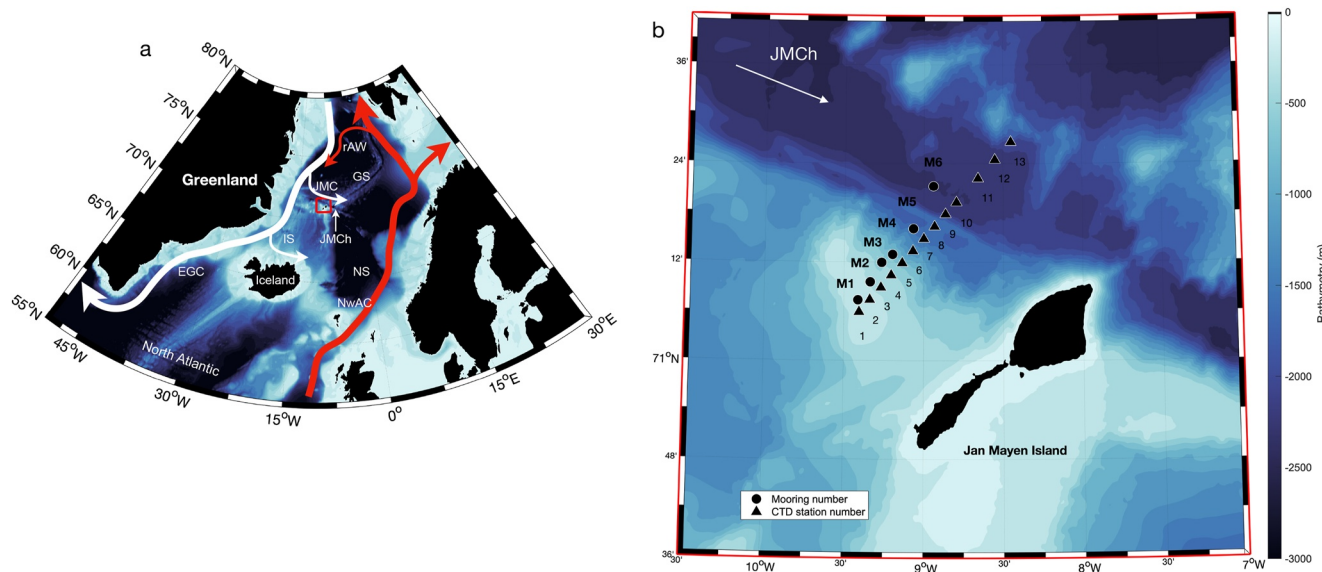
Figure 1. (a) Bathymetry of the Nordic Seas (in m). Arrows summarize the main branches of the circulation, with the warm surface currents of Atlantic origin in red and cold fresher surface currents of Polar origin in white. Abbreviations: rAW is return Atlantic Water, GS is Greenland Sea, JMCh is the Jan Mayen Channel where the JMC (Jan Mayen Current) circulates, IS is the Iceland Sea, NS is the Norwegian Sea, NwAC is the Norwegian Atlantic Current and the East Greenland Current (EGC) is the EGC. (b) Location and names of the moorings (black dots) and CTD stations numbers (triangles) in the Jan Mayen Channel.

consists of the JMCh and other numerous pathways and gaps in the mid-ocean ridge (Brakstad et al., 2023; Swift & Koltermann, 1988; Wang et al., 2021). However, the knowledge about these pathways allowing deep and intermediate Greenland waters to be exported to the Norwegian Sea is still incomplete despite its importance. For instance, up to 50% of the freshwater transferred from the surface-intensified EGC to the interior of the Nordic Seas might occur via the JMCh within the Jan Mayen Current (JMC; Bourke et al., 1992), whose intensity has been observed to be around 0.5–1.6 Sv (Shao et al., 2019; Wang et al., 2021). Providing a description of the JMC, sampled in the JMCh, is the main objective of this paper.

Two key elements have classically been considered when investigating the variability in the volume of NSDW and the transport into the channel: (a) the variability in deep convection in the Greenland Sea, and (b) the sea ice conditions in the Greenland Sea (e.g., Lauvset et al., 2018). However, both these features have drastically changed recently (Brakstad et al., 2019; Khosravi et al., 2022; Lauvset et al., 2018), and are expected to change further in the future (Lique & Thomas, 2018; Lique et al., 2015), as the Greenland Sea is predicted to be a hotspot of climate change (Khosravi et al., 2022). Among the substantial changes that have already been observed in the region, the warming of the deep waters (GSDW shows a linear warming trend of 0.13°C decade^{-1} between 1982 and 2010; Somavilla et al., 2013) and the reduction in the deep water formation in the Greenland Sea (Dickson et al., 1996) are of major concern and have the potential to impact the circulation in the Nordic Seas and beyond. Consequently, since the 1970s, convection in the Greenland Sea did not reach very deep anymore and has only been observed at intermediate depths (i.e., above 2,000 m), thus forming a slightly warmer and dense Greenland Sea Arctic Intermediate Water (GSAIW) rather than GSDW. Brakstad et al. (2019) further show that GSAIW is presently the dominant water mass of the upper 2,000 m of the Greenland Sea. The sea ice conditions have also changed drastically over the past decades. The outstanding example of this is the Odden ice tongue that used to cover all, or part, of the area of influence of the JMC in winter (Comiso et al., 2001; Wadhams, 1981; Wadhams et al., 1996), as it developed across the southern part of the Greenland Sea, extending eastwards from the EGC. The extent of the Odden ice tongue was suggested to modulate the intensity of the deep convection in the Greenland Sea (Germe et al., 2011). However, the Odden ice tongue has not formed anymore since the early 2000s (Comiso et al., 2001), suggesting that other drivers are now at play to trigger the development of deep convection in the region.

Despite its essential role in maintaining an overflow between the Greenland and the Norwegian Seas, the circulation in the JMCh is still poorly quantified and understood. Most of the previous studies have focused on the Jan Mayen Ridge and frontal system, south of the JMCh (Mork et al., 2014). The few existing studies focusing on the

JMCh have two main limitations: (a) they rely on observations from the 1980's when the conditions in the region were probably very different (Swift & Koltermann, 1988), and/or (b) they are limited to very short time scales, that are not long enough to provide a consistent description of the current mean state and its variability in this region (Wang et al., 2021). These studies pointed out that direct measurements over an extended period of time are needed (Mork et al., 2014; Shao et al., 2019; Wang et al., 2021). So far, details on circulation and water mass transport between the two basins via the Jan Mayen Channel are still lacking.

One major and striking feature previously highlighted in the literature is the cessation and/or the reversal of the deep flow, below 1,200 dbar, in the channel at some times (Østerhus & Gammelsrød, 1999; Wang et al., 2021). This reversal has been historically documented and observed during relatively long periods of time (of the order of 9–12 months; Østerhus & Gammelsrød, 1999) and may have the potential to impact the circulation and the properties of the two adjacent basins. For example, this reversal is thought to be at the origin of the different warming rates of the deeper water masses in the Norwegian and the Greenland Seas over 1950–2000 (Østerhus & Gammelsrød, 1999). Several explanations have been put forward for these reversals of the flow. Østerhus and Gammelsrød (1999) found that the intensity of the flow within the channel is related to the density distribution at depth in the Greenland and Norwegian Seas and thus depends on the equilibrium between the two. The channel would thus act as a corridor with water flowing toward the Norwegian Sea when the density is higher on the Greenland side and vice versa. Consequently, the reversal of the flow in the JMCh was ascribed to the minimum reached in the Greenland Sea convection (Bigg et al., 2005; Turrell et al., 1999).

Although observed, the identification of this reversal in early data sets may be associated with poorly resolved observations. It is also not clear if such events would still occur in the most recent ocean and sea ice conditions found in the Nordic Seas. The appearance, the frequency and duration of this reversal are still unclear. A new framework is needed to document the recent conditions of JMC and thus the southernmost part of the Greenland Sea Gyre. Conditions for water mass circulation through the channel may be related to density distribution but also to regional and local hydrographic, atmospheric and sea ice conditions.

Using direct temperature, conductivity and current measurements from a yearlong mooring array between summers 2017–2018 along 71–72°N/9.5–8.3°W over the JM Ridge slope, we seek a new comprehensive description of the circulation of the JMC at the entrance of the JMCh, and its associated variability. We first present the data set and methodology used for the study in Section 2. Section 3.1 describes the mean state of the JMC based on Conductivity-Temperature-Depth (CTD) data and the 2017–2018 yearlong mooring data. Then, the variability on several time scales (annual, seasonal and daily) are discussed in relation to atmospheric forcing as well as the impact on the larger circulation in the Nordic Seas (Section 3.2–3.4). Discussion and conclusions are given in Section 4.

2. Data and Methods

2.1. Mooring Array and Instrumentation

We use data from a mooring array deployed from 29 August 2017 to 01 August 2018 across the slope in the vicinity of Jan Mayen Island in the Greenland Sea (Figure 1). The array consisted of six moorings (labeled M1-M6, progressing onshore to offshore) and spanning a distance of ~30 km centered at 71.2°N and 9.2°W. The moorings were deployed in water depths of 170–1,982 m and their designs are presented in Figure 2. The various instruments mounted on the moorings are listed in Table 1.

Upward-looking Acoustic Doppler Current Profilers (ADCP) of various frequencies (ADCPs 75, 190, 250, and 400 kHz) provide velocity profiles. The vertical resolution is ranging from 6 m (on M1, M2, and M5) to 16 m (on M4) in the upper 500 m and sampling intervals vary from 30 min (on M1) to 60 min (on M2, M4, and M5). In addition, point measurements of velocity are obtained from Nortek Aquadopp instruments (2 MHz) mounted on the two most offshore moorings (M5 and M6).

Temperature (*T*) observations are obtained from Sea-bird Electronics (SBE) SBE-39 sampling every 4 min and SBE-37 sampling every 1.5 min. Salinity (S) observations come from SBE-37 only. All SBE instruments also provide pressure observations. In the upper layer (0–400 m), temperature and salinity data were obtained at varying vertical resolution of ~60–530 m and 100–250 m respectively. However, M3 and M4 were not instrumented for salinity. All the hydrographic variables (potential temperature, salinity, potential density) were first quality controlled against the CTD profiles conducted from the ship at the mooring's deployment location and time.
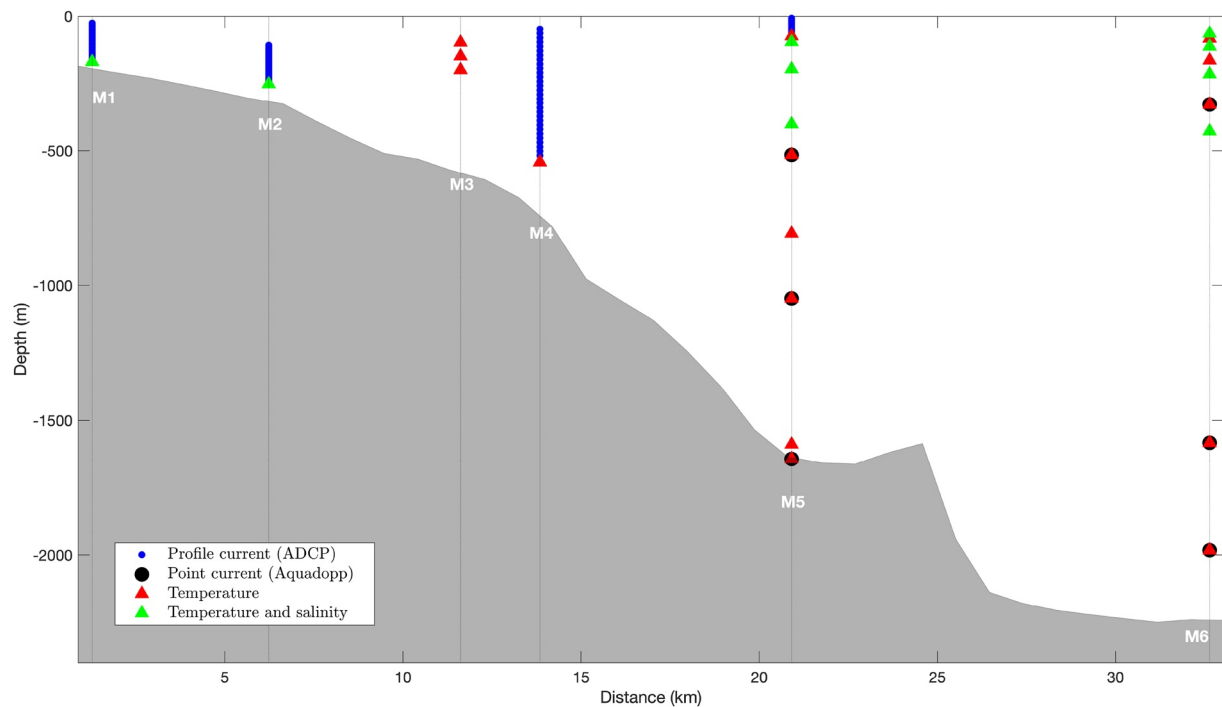
Figure 2. Cross-section of the mooring array on the continental slope around Jan Mayen Island and instruments deployed on each mooring. Depths of *T* instruments are identified by red triangles, and *T/S* instruments are shown as green triangles. The black dots correspond to the Aquadopp instruments and the blue dots are the levels of the velocity data provided by the ADCPs that look upward. *X*-axis is the distance along the section in km, the origin being the M1 location minus 400 m.

Prior to deployment and after their retrieval, all the SBE instruments were calibrated by SHOM (Service Hydrographique et Océanographique de la Marine, France). Once calibrated, the accuracy of the data is estimated to be $\pm0.002°C$ in temperature and ±0.02 psu in salinity. The ADCP precision and resolution are reported by the manufacturer to be 3% of measured value and ±0.01 cm·s^{-1} respectively. All instruments were recovered during the turnaround in August 2018 and overall, the data return was very good. Only tree instruments failed during the deployment period: one SBE-37 on M3 was removed from the analysis as the temperature time series showed a large drift over time, and two SBE-37 on M6 stopped recording after 2 months (for SBE-37 at 65 m deep) and 8 months (for SBE-37 at 216m deep) in the water.

This mooring array was initially designed to be deployed in the seasonally sea ice covered region close to the Greenland coast, which explains why the moorings are lacking instruments in the upper layer of the water column, where they would have been at risk of being ripped off by sea ice and icebergs. Due to meteorological and sea ice conditions during the cruise, the initial deployment plan was not possible and the moorings were finally deployed as introduced here.

2.2. Processing of Moored Data

All current meters were corrected for magnetic declination. Declination is calculated using the NOAA's magnetic field calculator. A constant magnetic declination was chosen for the whole year, as the declination was changing by less than 0.36° over the year. For the studied array, the declination is 9.55°.

Velocity fields *u* and *v* were rotated into along channel (u_{along}) and across channel (v_{across}), that is, perpendicular and parallel to the mooring array respectively. The convention in this study is that positive u_{along} corresponds to a current directed from the Greenland Sea to the Norwegian Sea and positive v_{across} corresponds to a current directed from M1 to M6 (offshore).

A third-order Butterworth filter with a cutoff period of 2 days was used to extract signals from tides and inertial oscillations from all data records (i.e., temperature, salinity, velocity), and then data are hourly averaged. This method does not affect the low frequency variance content.

Table 1
Mooring and Instruments Information Used in the Present Study

Mooring Longitude Latitude Bottom depth	Type, variable	Instrument depth (m)	Time step (s)	Note
M1	SBE 37 (T, S)	170	90	
9°41.22°W	250 kHz ADCP (u, v)	170	1,800	Removal of u and v < 75 m
71°12.34°N				
170 m				
M2	SBE 37 (T, S)	252	90	
9°33.57°W	190 kHz ADCP (u, v)	252	3,600	Removal of u and v < 120 m
71°15.98°N				
252 m				
M3	SBE 39 (T)	99	240	
9°26.44°W	SBE 39 (T)	149	240	
71°19.94°N	SBE 39 (T)	200	240	
547 m				
M4	75 kHz ADCP (u, v)	542	3,600	Removal of u and v < 60 m
9°19.61°W				
71°21.58°N				
547 m				
M5	400 kHz ADCP (u, v)	86	3,600	
9°06.54°W	SBE 37 (T, S)	96	90	Removal of u and v < 10 m
71°26.78°N	SBE 37 (T, S)	197	90	
1,649 m	SBE 37 (T, S)	401	90	
	2,000 kHz Aquadopp (u, v)	516	1,800	
	SBE 39 (T)	807	240	
	2,000 kHz Aquadopp (u, v)	1,049	1,800	
	2,000 kHz Aquadopp (u, v)	1,590	1,800	
	SBE 39 (T)	1,643	240	
M6	SBE 37 (T, S)	65	90	Record stops on 29 October 2017
8°94.07°W	SBE 39 (T)	83	240	
71°35.42°N	SBE 37 (T, S)	113	90	
2,232 m	SBE 39 (T)	164	240	
	SBE 37 (T, S)	216	90	Record stops on 26 April 2018
	2,000 kHz Aquadopp (u, v)	328	1,800	
	SBE 37 (T, S)	428	90	
	2,000 kHz Aquadopp (u, v)	1,582	1,800	
	2,000 kHz Aquadopp	1,982	1,800	

In order to quantify the net volume transport across the array (Section 4), data matrices of potential temperature, salinity, along and across section velocity that are consistent in space and time are needed. As such, hourly vertical sections of the hydrographic variables and velocity were interpolated using a simple linear interpolation with a regular grid spacing of 1 km in the horizontal and 5 m over the vertical. The linear interpolation returns no value where we do not have in-situ data, which explains the blanks in the sections (Figures 6 and 7). Although

Table 2
Main Water Masses Found in This Study and Defined From These Data, Swift and Aagaard (1981), Shao et al. (2019), and Wang et al. (2021)

Water masses	Potential temperature (°C)	Salinity	Distinction
Arctic surface water—ASW	$T > 0$	$34.4 < S < 34.7$	
	$T > 2$	$34.7 < S < 34.9$	
Polar Water—PW	$T < 0$	$S < 34.4$	Cold PW
	$T > 0$	$S < 34.4$	Warm PW
Polar Intermediate Water—PIW	$T < 0$	$34.4 < S < 34.7$	
Forms a temperature minimum underneath the upper waters of the East Greenland Current			
Arctic Intermediate Water—AIW	$T < 2$	$34.7 < S < 34.9$	Upper AIW
Water formed in the Arctic domain in the Iceland and Greenland Seas			
Return Atlantic Water—rAW	$0 < T < 2$	$34.9 < S < 35$	
Water of Atlantic origin that has circulated into the East Greenland Current from the West Spitsbergen Current and the Atlantic layer in the Arctic Ocean			
Norwegian Sea Arctic Intermediate Water—NSAIW	$-0.5 < T < 0.5$	$34.87 < S < 34.9$	
Water advected from the Greenland and Iceland Seas that has a salinity minimum in the Norwegian Sea			
Greenland Sea Arctic Intermediate Water—GSAIW	$-0.5 < T < 0$	$34.9 < S < 34.92$	
Water produced by open-ocean convection in the Greenland Sea Gyre. Densest intermediate water in the Nordic Seas			
Norwegian Sea Deep Water—NSDW	$T < -0.5$	$34.9 < S < 34.94$	
Distributed around the periphery of the Greenland Sea Gyre including the area in the southern Greenland Sea. Densest water in the Norwegian Sea			
Greenland Sea Deep Water—GSDW	$T < -1$	$34.88 < S < 34.9$	
Densest water mass in the Greenland Sea and only found in the central gyre of Greenland Sea			

simple, the linear interpolation performed here has the advantage of not introducing unrealistic signals to satisfy some limit conditions. To produce these monthly mean sections, we only focus on the top 0–430 m where the density of data is higher and where most of the variability occurs. Error associated with the interpolation method, the spatial sampling and the instrumental uncertainties is discussed in Appendix A.

The seasonal and total variances are computed for the period 2017–2018. The ratio between the two (i.e., seasonal variance/annual variance) corresponds to the explained variance and allows us to analyze the spatial patterns and magnitude of the intra annual variability.

2.3. CTD Data and Main Water Masses Sampled at the Array

Our moored observations are compared against the CTD section completed during the deployment and along the mooring array in August 2017, from the R.V. Pourquoi Pas?, sampling 13 stations along the mooring array. The CTD station numbers are displayed on Figure 1. The CTD observations show the general hydrographic features found in the channel and are used to define the major water masses covered by this study (see Table 2). The water masses in the Nordic Seas were first classified by Swift and Aagaard (1981) and the classification has been updated more recently to take into account the recent changes associated with the continued warming and salinification of the Greenland Sea (Kasajima & Johannessen, 2009; Shao et al., 2019).

We also compute the geostrophic velocity across the CTD section and from direct velocity observations. The common way to obtain a profile of geostrophic velocity from a hydrographic profile is to vertically integrate the thermal wind balance from a reference level (usually the deepest observed). Here, the deepest CTD casts do not correspond to a level of no motion. Rather, we use as a reference the annual mean velocities directly measured
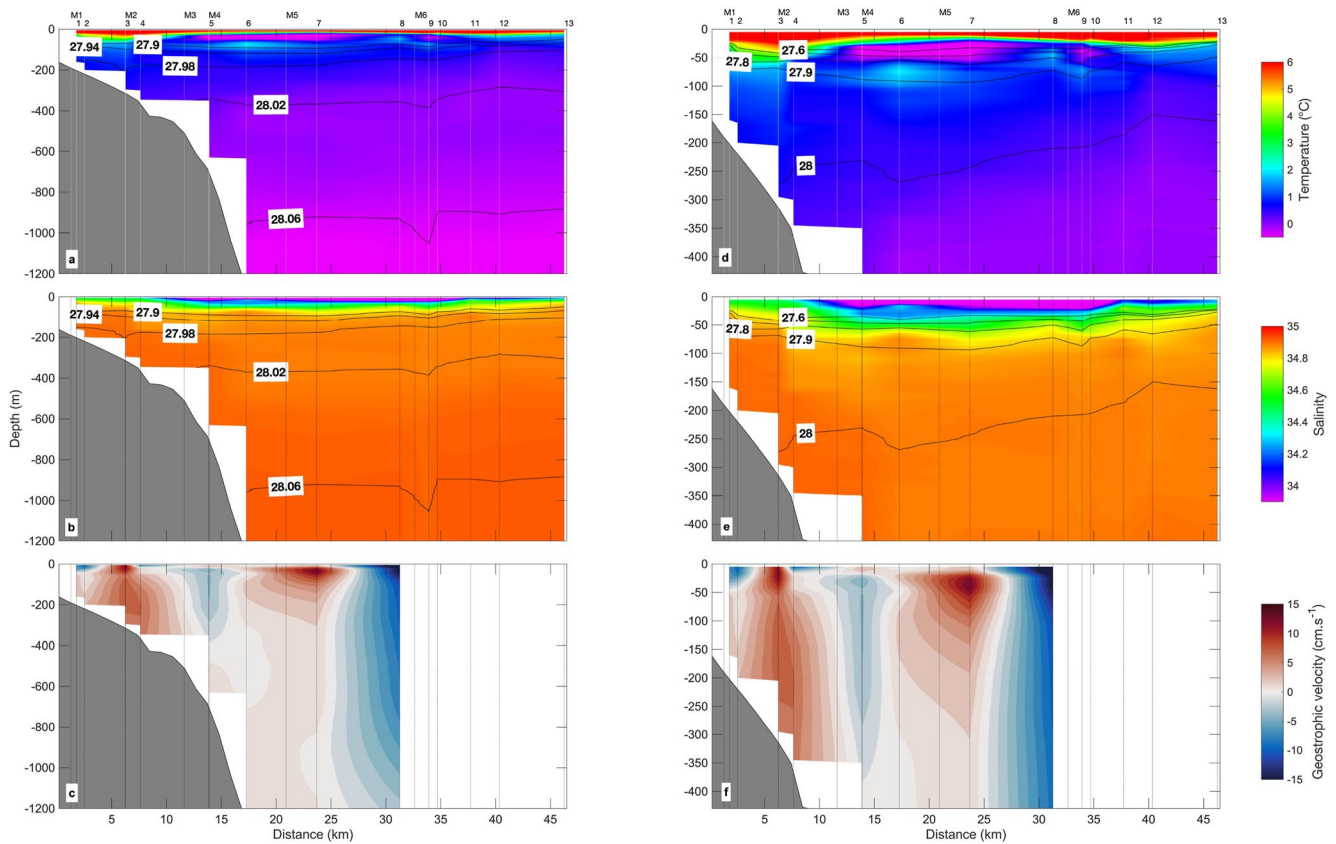
Figure 3. CTD section over 0–1,200 m (left) and a zoom over 0–430 m (right) of potential temperature (a and d) and salinity (b and e) performed at the deployment of the mooring in August 2017. The black contours are isopycnals. Estimated geostrophic velocity (cm·s^{-1}) structures are shown in (c and f). We mask the geostrophic velocity section beyond the M6 position where we do not have any Acoustic Doppler Current Profilers data to use as reference level. The numbers on the top x-axis indicate locations of CTD stations and moorings as displayed in Figure 1.

by the closer ADCP located on the moorings at the closest depth from the deepest CTD measurements. The ADCP—referenced geostrophic velocity across Appendix A is estimated as following:

$$f\frac{\partial V}{\partial z} = -\frac{g}{\rho_0}\frac{\partial \rho}{\partial x}$$

(1)

where f is the Coriolis parameter, g is the gravity acceleration and x is the coordinate along the CTD section.

2.4. Atmospheric Data

In order to assess the large-scale atmospheric conditions at the mooring location and to investigate the relationships between the currents and winds, we use hourly wind data from the ERA-5 reanalysis (Hersbach et al., 2020, 2023). This hourly wind product comes from the European Center for Medium-Range Weather Forecasts (ECMWF) and has a spatial resolution of 0.25°.

3. Results

3.1. Mean Conditions

A snapshot of the hydrographic conditions from the CTD section conducted on 29 August 2017 gives us an overview of the section at the entrance of the channel from top to bottom. Across the JMCh, the waters on the shelf and those in the center of the channel are quite different (Figure 3). This distinction between shelf and channel waters is very noticeable in the T-S space (Figure 4) that shows the distinct characteristics of the surface layer on the shelf (stations 1 to 4) and in the channel (stations 5 to 7).
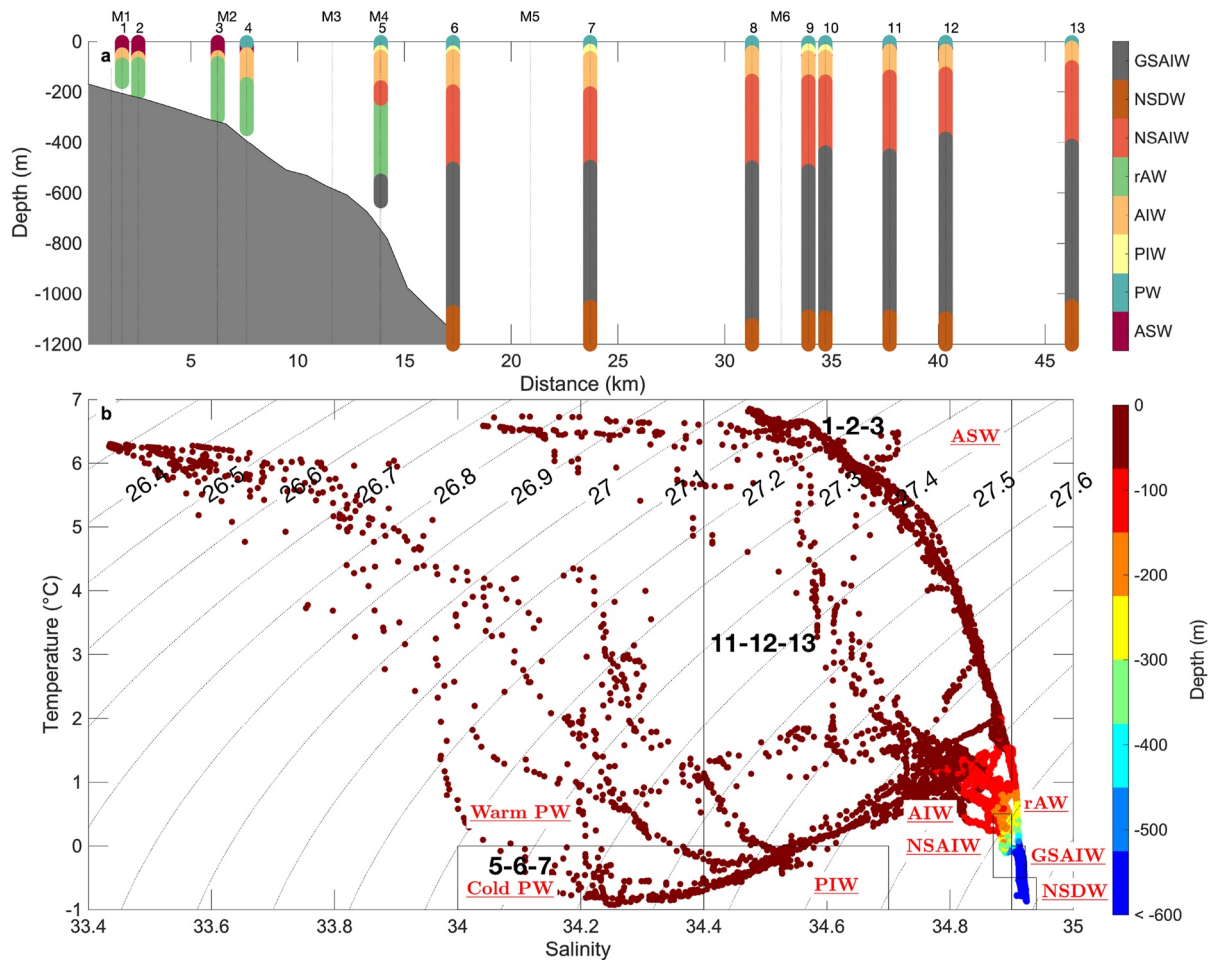
Figure 4. The main water masses found in the channel are represented in (a) with the abbreviations as defined in Table 2: GSAIW, Greenland Sea Arctic Intermediate Water; NSDW, Norwegian Sea Deep Water; NSAIW, Norwegian Sea Arctic Intermediate Water; rAW, return Atlantic Water; AIW, Arctic Intermediate Water; PIW, Polar Intermediate Water; PW, Polar Water; ASW, Arctic Surface Water. The numbers on the top *x*-axis indicate locations of CTD stations and moorings. The lower panel (b) shows the distribution in *T-S* space with overlaid depth and number of several CTD stations.

Shelf waters (i.e., centered on CTD stations number 1 to 4 and M1–M2) are warmer and saltier than these at the center of the channel. The shelf is well stratified, with temperatures between 2 and 7°C and salinity ranging from 34.4 to 34.9 between 0 and 50 m depth. This corresponds to Arctic Surface Water (ASW) that forms after Polar Water from the EGC mixes with saltier Atlantic Water and that is highly influenced by precipitation and solar radiation (Shao et al., 2019; Swift & Aagaard, 1981). Below the ASW, we find AIW as well as a water mass following the continental slope with high salinity (higher than 34.9) and positive temperatures (0–2°C) which is referred to as return Atlantic Water (rAW; Fogelqvist et al., 2003; Shao et al., 2019). This warm and saline water mass, only found on the shelf and continental slope, is of Atlantic origin and has likely circulated within the EGC before reaching the JMCh region (Fogelqvist et al., 2003; Shao et al., 2019).

In contrast, the surface layer in the channel (i.e., centered on CTD stations number 5 to 7 and M4–M5–M6) is about 1 unit fresher than on the shelf. There, the pycnocline rises near the surface because of the presence of a cold and fresh core ($S \sim 34.2$ and $T < 0$°C) visible in the sub-surface around 50 m, that caps slightly warmer and saltier waters centered at 100 m ($S \sim 34.8$ and $T \sim 1$°C). This destabilizing temperature gradient is due to the presence of Polar Water (PW) that was absent on the shelf. PW is carried into the Nordic Seas by the EGC and thus exhibits lower salinities ($S < 34.4$) due to sea ice melt in the Arctic region. The PW are divided into warm PW ($T > 0$°C) at the very top of the water column overlying the first cold and fresh core of cold PW at 50 m ($T < 0$°C). Then, the deeper, warmer and saltier core at 100 m is likely AIW as defined by Swift and Aagaard (1981) and Blindheim (1990).
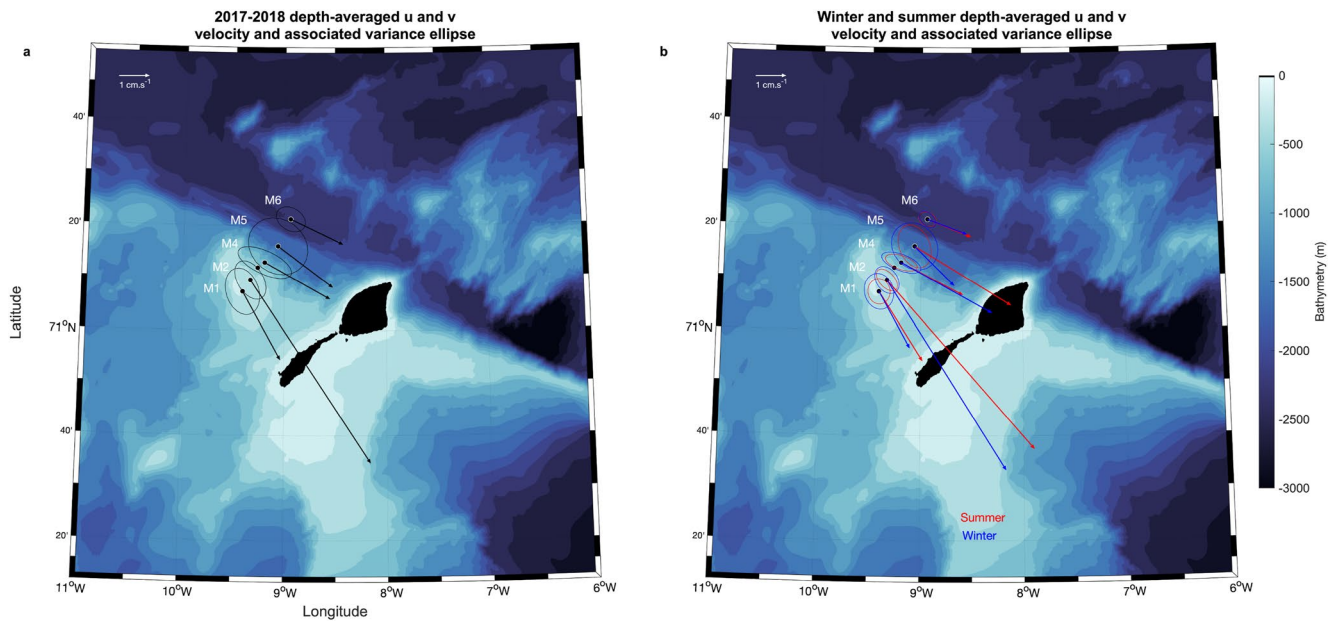
Figure 5. Vertically averaged velocity vectors at the mooring sites together with their variance ellipses for (a) the 2017–2018 yearlong time series and (b) summer in red versus winter in blue. The bathymetry (in m) is shading according to the colorbar. M3 is not displayed as it does not have velocity measurements.

Below 100 m depth, while the shelf is composed of a salty tongue of rAW, the channel contains three major water masses: NSAIW between 150 and 300 m in the range 34.87–34.9 and −0.5–0.5°C (Kasajima & Johannessen, 2009; Swift & Aagaard, 1981), GSAIW from ~300 to 1,000 m and NSDW below 1,000 m in the range 34.9–34.94 and less than −0.4°C (Fogelqvist et al., 2003; Swift & Aagaard, 1981).

We start our analysis of the mooring data set by presenting the yearlong mean structure of the velocity across the mooring array. Figure 5a shows the 2017–2018 full depth-averaged velocity vectors along with the variance ellipses at each mooring site. Again, this reveals the different characteristics of the current on the shelf compared to the rest of the section. On average, the current is flowing southeastward along the topography of the channel at each mooring location. At M1, M4, M5 and M6, the currents averaged over 2017–2018 and over the entire water column are about 2.57, 2.47, 2.26, and 1.91 cm·s^{-1}, respectively. In contrast, the current on the shelf at M2 exhibits higher mean velocities, with a magnitude more than two times larger than the others (7.22 cm·s^{-1}; Figures 5 and 6). The variance ellipses show that the variability of the JMC is dominated by the along-channel variability of the velocity vector.

To understand the vertical structure of the flow, we examine the sections of the annual mean along and across channel velocity (u_{along} and v_{across}; Figures 6a and 6e), and compare it to the section of geostrophic velocity (across the section) estimated from the CTD cast at the time of the deployment (Figures 3c and 3f).

As mentioned earlier, M2 is located right in a persistent vein of an intensified current, on the shelf break (Figure 6a). This strong current is directed eastward that is, from the Greenland Sea to the Norwegian Sea, however, given the complex multi-path current system at this location, it is possible that all or part of this current bypasses the JMCh and is for example, constrained to flow South into the Iceland Sea. This along-channel velocity, advecting relatively warm water (Figure 7), has a strong positive velocity core with velocity reaching as high as 7 cm·s^{-1} both from the mooring measurements and the geostrophic velocities, attached to the slope around the 400 m isobath. The signal is also associated with a local intensification of the across-channel velocities, reaching as high as 3–4 cm·s^{-1} and are directed toward the shelf. The 2017–2018 total variance associated with this vein of current is relatively weak suggesting that the current pattern is largely stable over the 2017–2018 year. Due to the lack of instruments in the surface layer, the moorings do not sample the surface structure of this vein and it may be possible that this structure is not limited at 120 m depth but instead extends to the surface, as suggested by the geostrophic velocity section derived from the CTD section (Figure 3f). The geostrophic velocity section also reveals the presence of a second branch of current offshore, with a maximum around 10 cm·s^{-1} and an extension down to 200 m. The spatial sampling of the mooring array does not allow detection of this offshore branch.
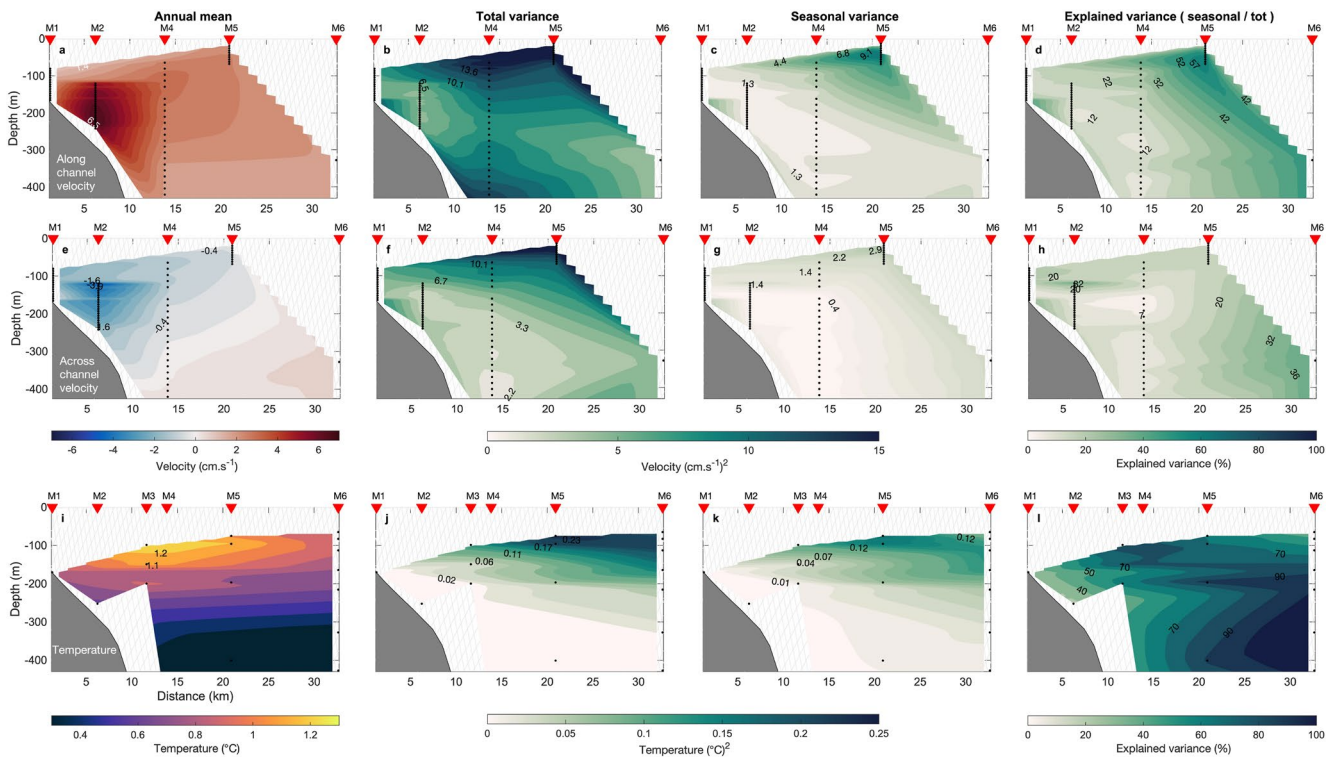
Figure 6. From left to right is the annual mean, total variance, seasonal variance and the explained variance (i.e., ratio between seasonal and total variance) for the u_{along} velocity (a–d), v_{across} velocity (e–h) and the temperature (i–l). The linear interpolation returns a blank where there is no in situ data. We displayed the u_{along} and v_{across} velocity instead of u and v as the along-channel velocity (u_{along}) is later used for the volume transport across the section.

3.2. Seasonality

We then examine the variability of the depth-averaged currents and the properties on seasonal timescale. In winter (December–January–February), the mean current slightly shifts southward compared to summer (June–July–August) at M1, M2, and M5 (Figure 5b), while the direction remains constant at M4 and M6, toward the southeast and parallel to the local isobaths. While the winter ellipses are larger than those of summer, the mean current is overall smaller in winter except at M4.

Based on the monthly mean sections, we also compute the contribution of the variance of seasonal cycle to the 2017–2018 total variance for each parameter (Figures 6c, 6g, and 6k). The strong jet-like vein of current along the channel is stable over 2017–2018 and shows very small seasonal variations, which account only for 12%–22% of the total variability (Figure 6c). Further north in the JMCh, the seasonal variability is larger and explains up to 57% of the 2017–2018 total variability. In contrast, the across-channel velocity does not exhibit a pronounced seasonal cycle anywhere (Figure 6g), and the maximum seasonal variance is seen around M4 - M5 at 100 m.

The most significant seasonality is found for the temperature field (Figures 6i–6l). Both its seasonal variance and total variance show the same pattern of high variability in the upper 200 m, and the ratio between the two is higher than 60% everywhere except on the shelf (Figure 6l). The temperature on the shelf is therefore less variable than in the JMCh and the seasonal variability drives most of the 2017–2018 variability.

Although the design of the moorings does not allow for a monitoring of the surface layer, we further describe these seasonal variations of the temperature in the subsurface (i.e., below 100 m). During the 2017–2018 year, the isotherms were significantly tilted from onshore to offshore (Figure 7), revealing again warmer waters on the shelf in accordance with the CTD data. In summer (Figure 7d), a warm layer first develops onshore, probably due to the fact that the upper part of the water column is easier and faster to warm than the deeper part in response to a downward atmospheric heat flux during summer. Positive temperatures around 1–1.3°C are thus visible between 100 and 150 m. Then, at the end of fall (Figure 7a), a thick subsurface layer is centered around 150 m and reaches 1.6°C.
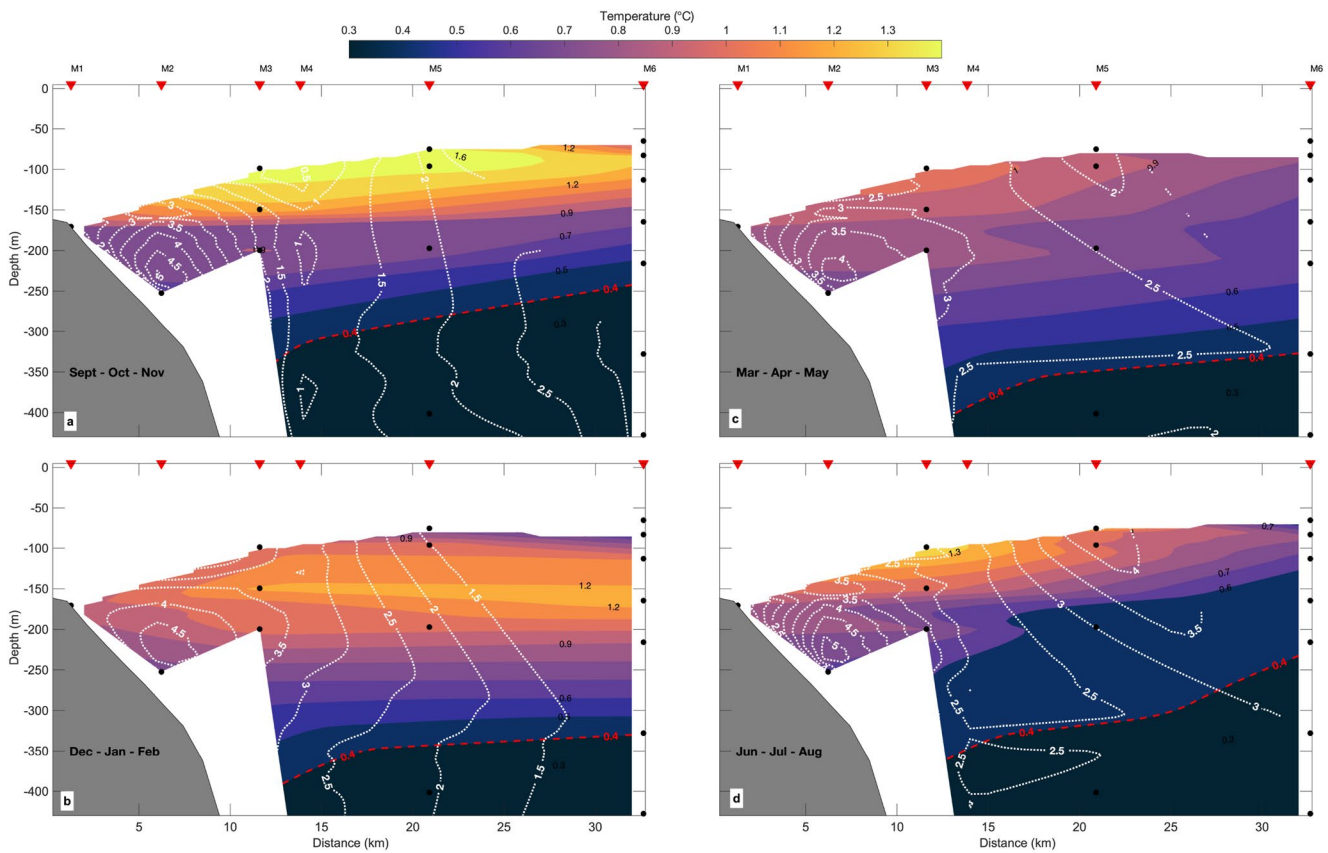
Figure 7. Seasonal sections of temperature (°C) at the mooring array for (a) fall, (b) winter, (c) spring and (d) summer. The red triangles are the locations of the moorings and the black dots are the levels of the temperature sensors. Contours of along-channel velocity (u_{along}, cm·s^{-1}) are in white. The 0.4°C isotherm discussed in the text is highlighted in red.

In winter, an interesting pattern of warming of the ocean interior is apparent (Figures 7b, 8c, 8d, 8g, and 8h), as depicted by for example, the deepening of the 0.4°C isotherm from 250 m (in fall) to 350 m (in winter), while the upper layer (100 m) is cooling. This relatively warm subsurface layer should be the remnant of the surface heat accumulated during summer and fall that deepens in winter as the mixed layer deepens. However, our results do not allow to capture the mixed layer depth and to confirm this hypothesis and it is also possible that a water mass of Atlantic-origin is advected above the moorings.

Our results reveal that the seasonal cycle of temperature is more pronounced offshore (Figures 6, 8b–8d, and 8f–8h) than on the shelf (Figures 8a and 8e). Even at comparable depths, the amplitude of the seasonal cycle in temperature of the shelf waters is about 0.4°C while it reaches almost 2°C in the JMCh. Indications of a similar behavior are found when examining the sparse salinity data. Moreover, the yearlong time series of temperature and salinity (Figure 8) highlight a decoupling between the variability in the subsurface (between 100 and 150 m) and deeper in the water column (200 m): when the subsurface reaches a temperature and salinity minima in winter (Figures 8b and 8f), the deeper layers reach their temperature and salinity maxima (Figures 8c, 8d, 8g, and 8h).

3.3. Variability at Higher Frequency

Although the temperature shows a strong seasonal contribution to the variability, the intensity and the structure of the current do not reveal a strong seasonality. This suggests that current variability is driven by processes occurring at higher frequency. Based on our results (Figures 6c and 6g), higher frequencies than seasonal may indeed dominate up to 80% of the JMC variability.

Daily current vectors are presented for several depths (Figure 9) allowing to estimate the intra-seasonal variability of the currents. A comparison between the wind at the surface and the current velocities is made to understand

Figure 8. Time series of (blue) temperature and (orange) salinity recorded at (a) M1, (e) M2, (b–d) M5 and (f–h) M6. The depth of the sensor is displayed in the right upper corner.

the surprising lack of seasonality in the 1-year measurements (Figures 6c and 6g). The time series of the wind from ERA-5 at the mooring array location shows no significant seasonal variation in the u and v components of the wind (Figure 9a). We found that only 34% of the annual wind speed variability is due to the 2017–2018 seasonal cycle. Instead, the surface wind exhibits high frequency variations in intensity and direction. This result is consistent with those from Mork et al. (2014), who also acknowledged the lack of seasonality in the local winds in the Jan Mayen region from 1956 to present.

Figure 9 demonstrates the different character of the current at M2 compared to the rest of the section. All the records show an average current direction toward the southeast, but the currents at M2 are the only ones exhibiting a very consistent southeast current with only very small variations in direction (slightly shift southward in winter). It is furthermore noticeable that the current at M2 never reverses northward, in contrast to the currents observed at the other moorings. This intense jet-like current at M2 is recorded over the entire sampled water column (from 120 to 242 m) and does not decrease neither with depth nor with time. This suggests the presence of a strong, permanent, largely barotropic and mainly unidirectional current at that location.

In contrast to M2, the other current data exhibit more variations in intensity and direction, including periods when the currents reverse direction. A different character of the currents in the channel (i.e., M5 and M6) and on the shelf (i.e., M1 and M4) is also noticeable from Figure 9. Although the number of reversals (defined as a sign change of both u and v i.e., from South-east to North-west) in the intermediate layer relative to the number of levels is comparable for all moorings (except for M2) and represents up to 6.7% of the 2017–2018 record at M6, 10.6% at M5, 11.9% at M4 and 11.3% at M1, the duration of these events is longer in the JMCh than on the shelf. Indeed, the longest reversal event of the current lasts for 11 days at M1 and M4 (at the deepest levels) and 22 days at M5 and M6 (both around 310–320 m depth).

In addition to these long-lasting reversals, the currents exhibit a number of shorter and larger events associated with a full rotation of the current direction, that last over 2–6 days. These transitions in the velocity fields could
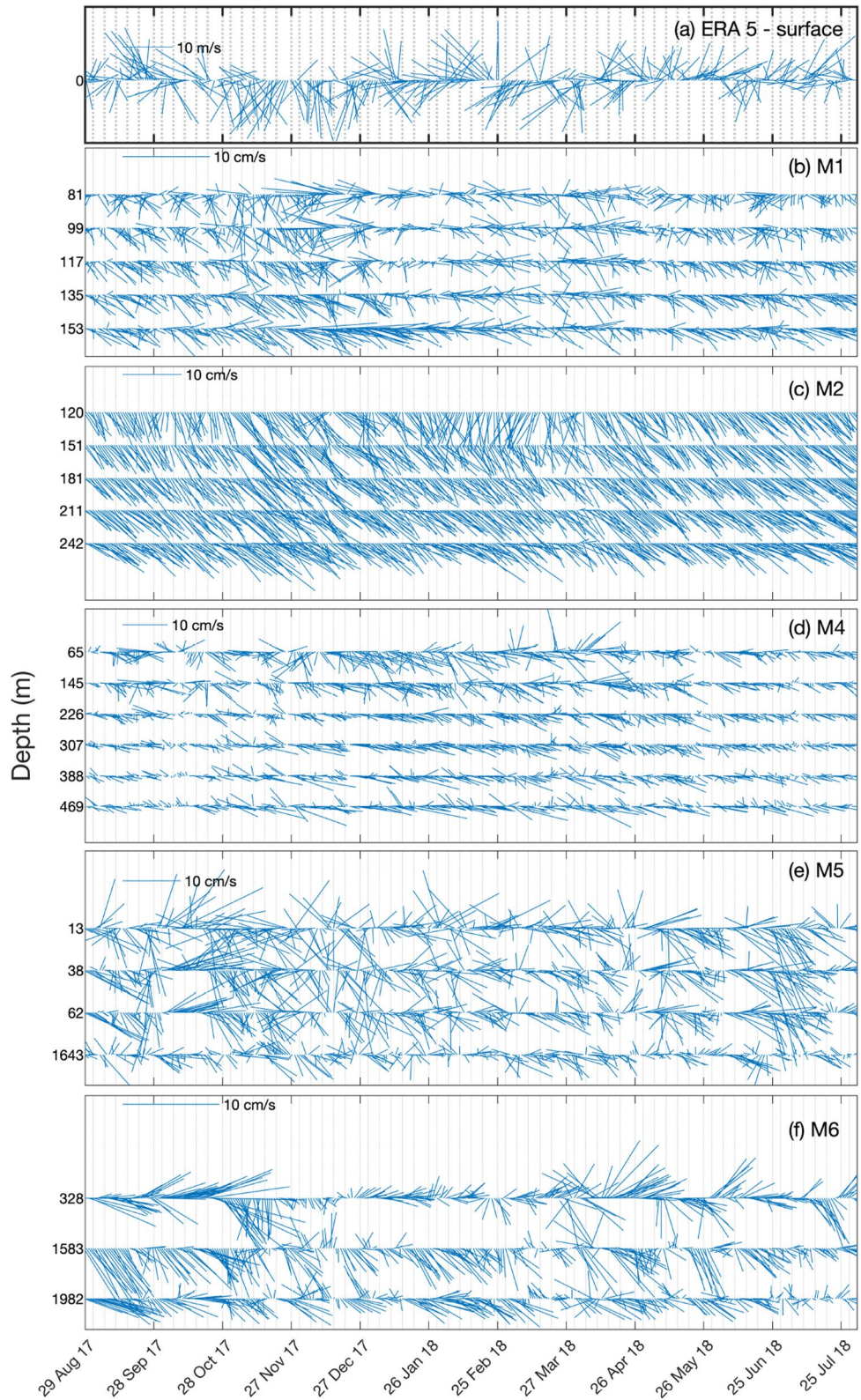
Figure 9. Daily stick plots velocity magnitude and direction from (b) M1, (c) M2, (d) M4, (e) M5, and (f) M6 at several depths indicated on the y left axis. Scale is different in each panel. The upper panel (a) are the wind daily vectors from ERA-5 reanalysis and averaged over the mooring array.
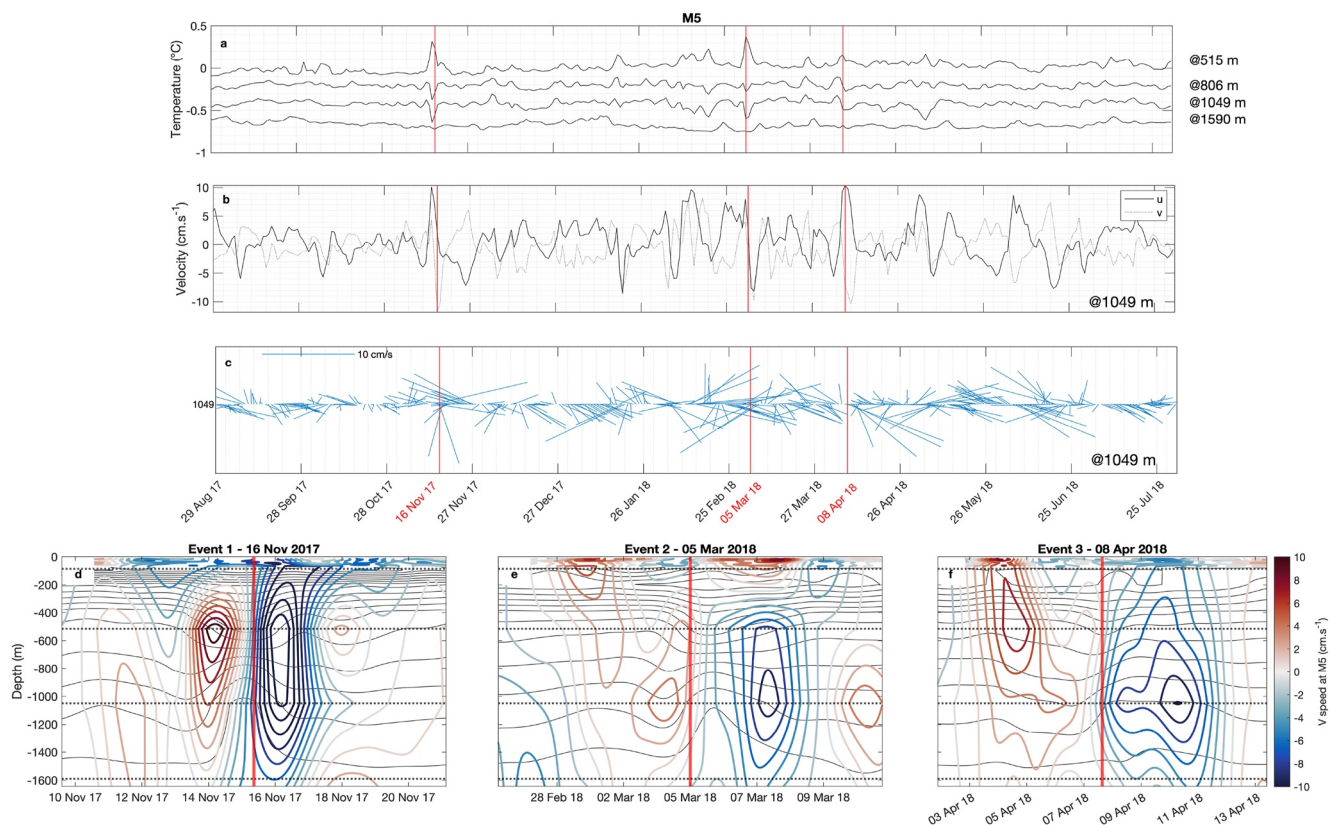
Figure 10. Short term events recorded at M5 during 2017–2018. (a) Time series of the potential temperature at 515, 806, 1,049 and 1,590 m. (b) Time series of u (thick) and v (thin) at 1,049 m and the associated daily stick vectors (c). Vertical red lines mark some of sudden rotations of the velocity that are discussed in the text and (d–f) are a zoom of potential temperature contours in black and v velocity in color around each of these events.

be the signature of mesoscale eddies passing through the mooring lines. Focusing on M5, which is both the deepest and the most equipped mooring for velocity, we notice that these abrupt events tend to be associated with temperature extrema (Figure 10a). Three events are particularly well marked, each of which is associated with a temperature anomaly over the entire water column, a velocity anomaly greater than 9 cm·s^{-1} and a rapid change in the direction of the current (Figure 10). Moreover, the temperature anomalies show a sign reversal between 500 and 800 m depth, related to a pinching of the isotherm, suggestive of (cyclonic) eddies.

Estimating the structure of a coherent eddy from a mooring may be a difficult task and our following description is thus limited to simple methods following Lilly and Rhines (2002). Making the assumption that the three eddies crossed the mooring at their centers and that they are advected by the background flow observed at the mooring (taken as the 10 - day average before the events, which is 1.97 cm·s^{-1} for event 1, 5.81 cm·s^{-1} for event 2 and 4.30 cm·s^{-1} for event 3), we make a back of the envelope estimate of the eddy properties. The temperature core of event 1 is localized around 600 m with a radius of roughly 1.7 km, while events 2 (centered at 1,000 m) and 3 (centered at 800 m) are much larger with radii of about 7 and 11 km respectively. These estimates are on the order of the first baroclinic Rossby deformation radius of about 4–6 km in this region (Nurser & Bacon, 2014). It is remarkable that the three eddies occupy a large portion of the water column, expanding from the surface down to 1,600 m. Moreover, the two first events are distinctly characterized by opposite temperature anomalies (Figure 10a) suggesting that they are cyclonic eddies. Although eddies are classically observed at the surface close to the slope intensified currents in this region from which they detached (e.g., Bashmachnikov et al., 2020), further analysis would be required to understand the formation location and associated mechanisms of these specific deep subsurface cyclonic eddies.

3.4. Variability in the Deeper Part of the Jan Mayen Channel

As mentioned in the introduction, Bourke et al. (1993) and Østerhus and Gammelsrød (1999) were the firsts documenting the deep reversal of the JMC circulation and conclude that the flow within the bottom of the JMCh
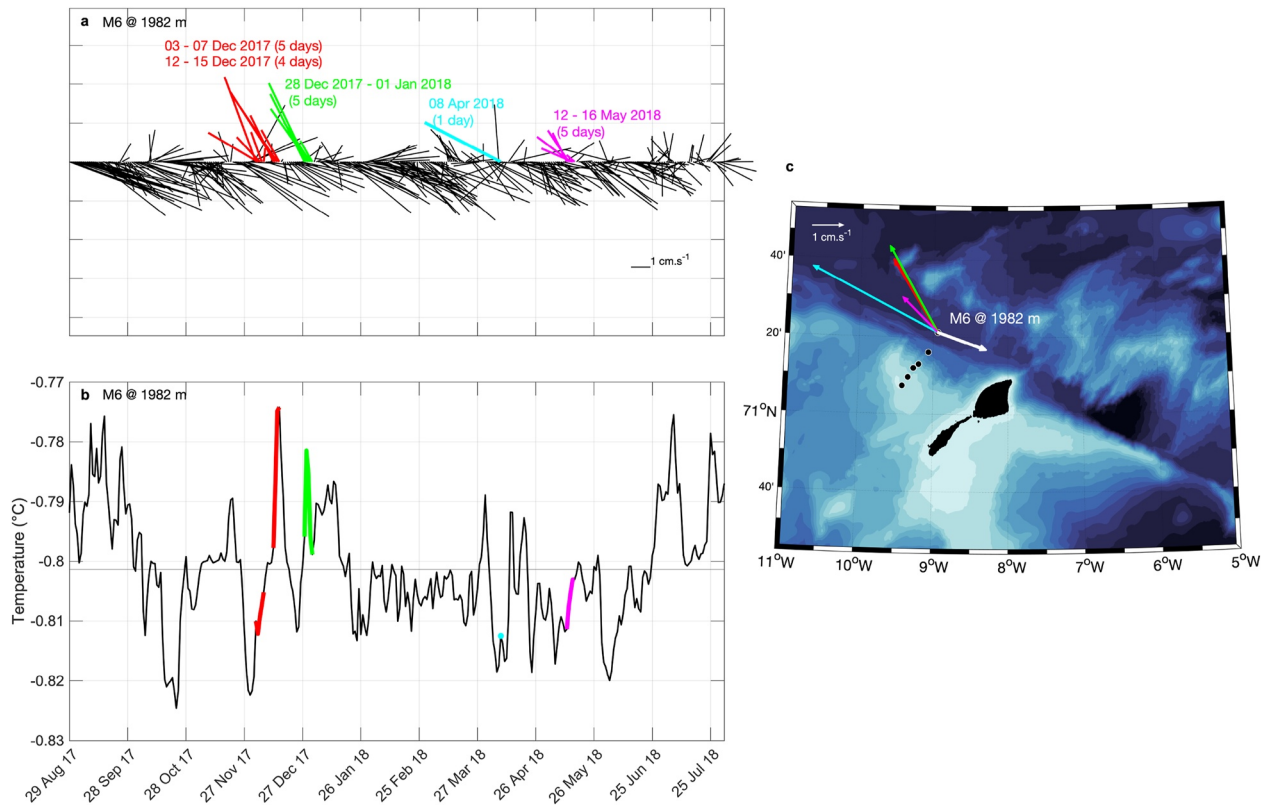
Figure 11. M6 deep reversals of the current. Time series of the velocity vectors (a) and temperature (b) at the deepest M6 Acoustic Doppler Current Profilers that is, 1,982 m depth. Colors highlight some of the short reversal events (defined as a sign change of both *u* and *v*) where the current shifts from the typical 2017–2018 South-East direction (i.e., white arrow on (c) which is the annual mean direction of the bottom current) to a North-West direction.

is intermittent on a time scale of a year or less. These studies thus questioned the importance of the JMCh in transporting water from the Greenland Sea to the Norwegian Sea below 2,000 m depth compared to other passages. As far as the intermediate layers are concerned, our study shows the significant role of this channel in transporting waters toward the Norwegian Sea. The deepest measurements from the mooring array, that is, the current meter fixed on M6 at 1,982 m, allows us to investigate the direction of circulation of the densest water mass in the JMCh over 2017–2018.

Figure 11 shows that the deepest current at M6 is largely flowing to the southeast, transporting waters from the Greenland Sea to the Norwegian Sea. The data present only very occasional JMC reversals deep into the channel. Some of these reversal events are also detected at upper levels (i.e., 1,582 m and 328 m). Besides eddies, if the reversal events appear in the whole water column, it could also be a typical barotropic disturbance by surface air pressure field driven by the wind field. Meanwhile, the reversal events only appearing at a certain level would be most likely the signature of a low frequency oscillation. Moreover, these reversal events do not necessarily imply a large flow into the Greenland Sea, as the duration of these events is short that is, from 1 to 5 consecutives days. The temperatures sampled at depth oscillate around −0.8°C, and do not exhibit any strong anomaly during the identified reversal events.

These temperatures are within the range of the temperature observed by Somavilla et al. (2013) at 2,000 m in the region (temperature range between −1°C in the 90's and −0.8°C in the 2000's) and by Bourke et al. (1993) in 1989–1990 at a comparable location in the JMCh and for the same depth range. Yet, the latter identified that the current sampled there was intermittent in a time scale of a year and less, at odds with our current observations which suggest a permanent current in the JMCh. Given the drastic changes that have affected the deep convection in the Nordic Seas since the observed reversal of the deep circulation (the latest observed one was in the early 1990's; Østerhus & Gammelsrød, 1999), one could expect that the state of the deep circulation presented in our study is more representative of the recent period, although the intermittency of the previously reported deep reversals makes it difficult to assess if such events are still occurring outside of our period of observation.

4. Discussion and Conclusions

Based on six moorings deployed between August 2017 and August 2018 north of Jan Mayen Island and across the continental slope, the vertical structure and variability of the JMC is documented for the first time over a full year. The data set offers a unique opportunity to quantify the variability of the currents and temperature of the southernmost branch of the Greenland Sea Gyre. Overall, we find that the JMC presents different behaviors on the shelf and in the channel.

From the 12-month time series, we find that the JMC at the entrance of the channel is characterized by a permanent current directed toward the southeast. Thus, over 2017–2018, the JMCh was a regular and direct route for intermediate and deep water from the Greenland Sea toward the Norwegian Sea. Examining the velocity structure through our section revealed the presence of a maximum located on the shelf in a jet-like structure with an intensity of about 7 cm·s^{-1}. Based on the hydrographic measurements from a campaign carried in 2015 in the same region, Wang et al. (2021) have documented a similar vein of current, albeit downstream east of the Jan Mayen Island, with maximum intensity of about 3 cm·s^{-1} centered around 200 m. However, in contrast to our results, they did not detect this vein of current at the entrance of the channel. They concluded that the downstream vein was probably related to a strong countercurrent further north and at the exit of the channel which forced waters inside the channel to come out. Our results rather suggest that this jet-like vein is a stable feature of the JMC as it is present all year round during the period covered by the moorings in 2017–2018. Moreover, we do not detect any westward water intrusion into the channel. These contrasted results may have several explanations. For example, this could reflect the fact that all the water transported by this jet-like vein does not circulate into the channel but instead is evacuated by the South and bypasses Jan Mayen Island by the South. Given the complex topography of the region (e.g., gaps, ridge, shelf), the strong current at M2 may indeed flow into the Iceland Sea. It is also possible that the limited length of their observational record (only a few days) is only capturing an intermittent structure that is not representative of a longer-term average circulation.

Contrary to some previous studies which highlight a reversal of the deep circulation in the channel over long periods (e.g., Østerhus & Gammelsrød, 1999 who documented a reversal of the circulation from November 1992 to July 1993), our data from the deepest mooring in the channel do not record such events; none of the moorings recorded a time-significant westward flow that would suggest a consistent feeding of the Greenland Sea by the Norwegian basin. If we want to document this current reversal, longer time series are necessary deep into the JMCh. In our records, some reversals occur at some occasions but these events remain really short.

We further investigate some short events during which the flow at intermediate depths reverses in the channel, and find that they are likely associated with eddies passing through the mooring array (although we cannot completely rule out that these events could be rather associated with the passage of propagating waves or eddy fluxes through ridges (Spall, 2010)). Consistently, it has been indicated that the exchanges between the Greenland, Iceland and Norwegian Seas are mainly associated with eddy shedding along the Arctic front separating the Greenland and Iceland Seas from the Norwegian Sea at the surface (Segtnan et al., 2011).

This intense circulation at the entrance of the JMCh and especially on the slope suggests that this branch of the Nordic Seas circulation could contribute to transport significant amounts of volume, heat and freshwater between the different basins, as suggested earlier by for example, Bourke et al. (1992). To gain insight on these integrated transports of volume and tracers, we make use of the u$_{along}$ through the full depth of the section, to produce an estimate of the transport across our section (Figure 12).

Although we acknowledge that the error associated with our time series might be important due to the uneven sampling across the section, the interpolation, and the fact that we do not take into account the top 100 m where the velocity could be the largest, we nonetheless find an average transport of 0.57 ± 0.05 Sv (mean ± standard error as computed in Appendix A) over 2017–2018 (Figure 12a). Up to 15% of this volume transport takes place on the shelf (M1–M2) in the jet-like structure. The total transport is comparable to previous estimates of the intensity of the JMC (0.5–1.6 Sv; Hawker, 2005; Shao et al., 2019; Swift & Koltermann, 1988). By dividing the volume transport into depth-layers (Figure 12b), we find that surface and intermediate layers highly contribute to the total volume transport in the JMCh. Indeed, the layers 0–350 m and 350–1,000 m that have respectively an averaged density of 27.87 kg·m^{-3} and 28.04 kg·m^{-3} (estimates based on the deployment CTD data), contribute up to 39% and 37% of the total transport. The bottom layer, below 1,000 m with an averaged density of 28.07 kg·m^{-3}, over which occurs the direct exchange between Greenland and Norwegian Seas, contributes to 24%. Moreover,
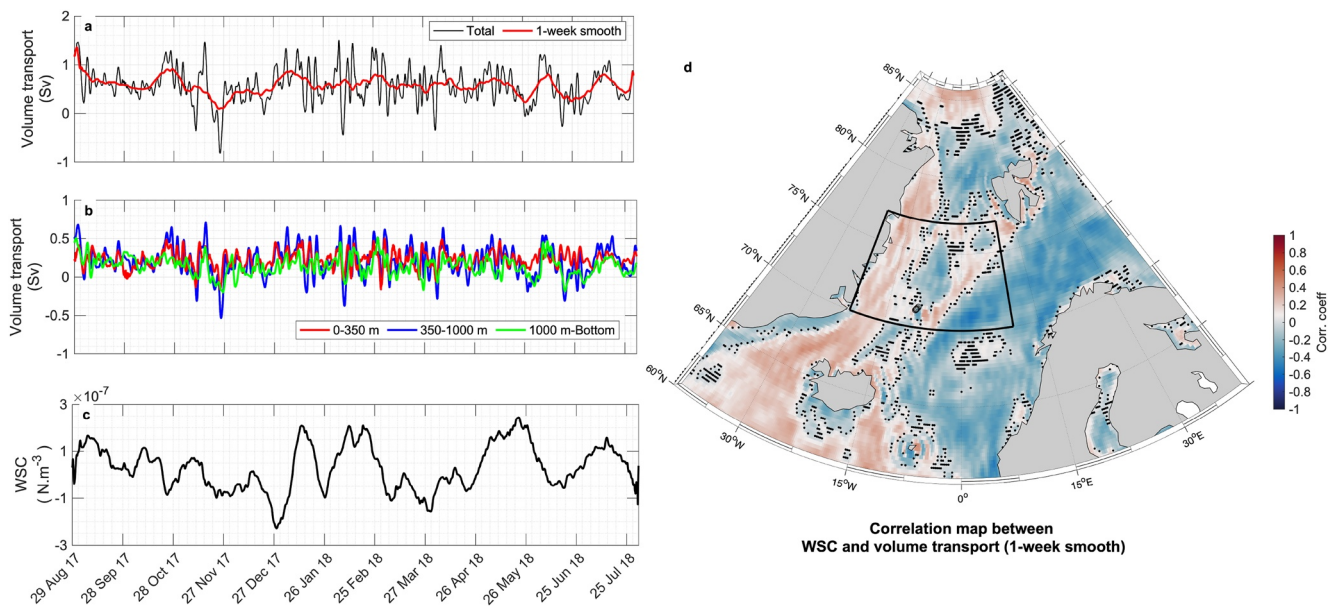
Figure 12. (a) 2017–2018 time series of the total volume transport estimated across the section (in black) and a 1-week smooth (in red). (b) Volume transport depending on depth classes. Red: 0–350 m; Blue: 350–1,000 m and Green: 1,000 to bottom. (c) Time series of the 1-week smooth wind stress curl (WSC) (N·m^{-3}) computed in the black box from (d). (d) Correlation map between the 1-week smooth transport of water across the mooring array and the 1-week smooth WSC. Stippling regions indicate the trends that are statistically not significant (*P*-value >0.05).

our volume transport estimate, and especially into the upper layer (0–300 m), may be a lower estimate due to the lack of measurement in the upper part of the water column.

Although our total transport estimate in the JMCh is consistent with previous ones, as explained in the introduction, numerous others pathways may exist for the Greenland water to enter into Norwegian Sea; water could be diverted either to the South around Jan Mayen or to the North along Mohn Ridge before entering the channel and/or water may enter JMCh without first passing through our mooring array. Not surprisingly, the transport does not exhibit a significant seasonal cycle, but rather shows variations at high frequency, similar to the variability of the velocity recorded by the different moorings. The lack of variability in the transport time series on synoptic time scales may suggest that the direct influence of passing low pressure systems is weak.

The JMC is part of the complex circulation of the Greenland Sea, so that its variability could partly be the signature of the large-scale variations in the intensity of the gyre. The barotropic gyre circulation is well known to respond to the overlying atmospheric forcing through WSC (Aagaard, 1970; Legutke, 1991) so that a positive WSC is found to drive a strong gyre index (and vice versa) over the central Nordic Seas (Chatterjee et al., 2018). To gain some hint of the larger scale forcing of the JMC variability, we estimate the correlation between the JMC transport time series and the WSC (estimated from the ERA-5 reanalysis; a 1-week running mean is also applied to the field prior to the correlation calculation). The correlation map is shown on Figure 12d. It reveals significant positive correlations in the Iceland Sea and all along the entire Greenland coast over the EGC. We also find negative correlations in the Norwegian Sea (correlation coefficients smaller than −0.6). In the Greenland Sea, we clearly discern the cyclonic pattern of the gyre that is highly correlated to the JMC, suggesting that the variations of this branch of current may be forced remotely at large scale over the Nordic Seas. Further analyses are required to fully elucidate the link between the variability in the properties of the JMC, the large-scale circulation and the potential for deep convection to occur in the Greenland Sea. Understanding the mechanisms at play is even more crucial at a time when large changes are occurring in this region and are expected to intensify in the future.

Appendix A: Uncertainties of the Volume Transport Calculation

Sources of errors in the volume transport mainly arise from ADCP instrumental errors (i.e., sensor accuracy), spatial sampling and interpolation method to fill the gaps.

Concerning the interpolation method, we choose a simple linear interpolation. Others methods were also tested to fill the gaps in the section, for example, (a) Laplacian interpolation and (b) using surface data (e.g.,

temperature/current) to create composite sections of each parameter, but the Laplacian interpolation tends to over-smooth the signal and it produces artifact signals at the surface due to ill constrained limit conditions, and (b) the products used to create a full data surface layer were not of comparable magnitude with the mooring data just below which again suggest a poorly known and resolved region. However, in order to estimate the bias caused by our interpolation method, we recomputed the velocity section using the nearest neighbor interpolation and the resulting transport. The volume transport is very close to the linear interpolation and the root mean square difference between the linear interpolation method and the nearest neighbor method is 0.02 Sv. The volume transport estimate is thus robust with regard to the interpolation method.

We estimated the uncertainty in the volume transport by constructing a 2D-matrix of error distribution of velocity that takes into account the instrumental error as well as the distance to the closest observation data point so that this uncertainty varies with depth and distance to the data point. This uncertainty section is constructed following the method of Koenig et al., 2022: (a) a nominal uncertainty estimate of the velocity measurements of 0.01 cm·s^{-1} at each mooring location, (b) one standard deviation of the observed velocity measurements at 4 km distance on both sides of the mooring and (c) two standard deviations of the observed velocity measurements mid-way between pairs of mooring. We choose the conservative value of 4 km as decorrelation scale as it corresponds to the Rossby deformation radius that is about 4–6 km in the region (Nurser & Bacon, 2014). The remaining gaps in the uncertainty matrix are filled by a linear interpolation. We ran 1,000 along-channel current sections by multiplying the average along-channel velocity section with the uncertainty section randomized with a white noise. We recompute 1,000 time series of the volume transport using these random fields. The error, estimated as the maximum amplitude of the variations of the volume transport obtained from these 1,000 simulations, is 0.05 Sv.

Data Availability Statement

Two data sources were used in this work and both are available online. The Jan Mayen mooring data (M1–M6) with data reference Narval Hydro 2017 (Balem & Pellichero, 2017) are available at https://doi.org/10.17882/90450. The wind data are from ERA5 (Hersbach et al., 2020, 2023), available at https://www.ecmwf.int/en/forecasts/datasets/reanalysis-datasets/era5. Finally, declination is calculated using the NOAA's magnetic field calculator freely available at https://www.ngdc.noaa.gov/geomag/calculators/magcalc.shtml.

References

Aagaard, K. (1970). Wind-driven transports in the Greenland and Norwegian Seas. *Deep Sea Research and Oceanographic Abstracts*, *17*(2), 281–291. https://doi.org/10.1016/0011-7471(70)90021-5

Balem, K., & Pellichero, V. (2017). Narval Hydro 2017 - Mooring dataset [Dataset]. SEANOE. https://doi.org/10.17882/90450

Bashmachnikov, I. L., Kozlov, I. E., Petrenko, L. A., Glok, N. I., & Wekerle, C. (2020). Eddies in the North Greenland Sea and Fram Strait from satellite altimetry, SAR and high-resolution model data. *Journal of Geophysical Research: Oceans*, *125*(7), e2019JC015832. https://doi.org/10.1029/2019jc015832

Bigg, G. R., Dye, S. R., & Wadley, M. R. (2005). Interannual variability in the 1990s in the northern Atlantic and Nordic Seas. *Journal of Atmospheric & Ocean Science*, *10*(2), 123–143. https://doi.org/10.1080/17417530500282873

Blindheim, J. (1990). Arctic intermediate water in the Norwegian Sea. *Deep Sea Research Part A. Oceanographic Research Papers*, *37*(9), 1475–1489. https://doi.org/10.1016/0198-0149(90)90138-l

Bourke, R. H., Paquette, R. G., & Blythe, R. F. (1992). The Jan Mayen Current of the Greenland Sea. *Journal of Geophysical Research*, *97*(C5), 7241–7250. https://doi.org/10.1029/92jc00150

Bourke, R. H., Paquette, R. G., Blythe, R. F., & Stone, M. D. (1993). On the deep and bottom waters of the Greenland Sea from summer 1989 and 1990 data. *Journal of Geophysical Research*, *98*(C3), 4629–4638. https://doi.org/10.1029/92jc02752

Brakstad, A., Gebbie, G., Våge, K., Jeansson, E., & Ólafsdóttir, S. R. (2023). Formation and pathways of dense water in the Nordic Seas based on a regional inversion. *Progress in Oceanography*, *212*, 102981. https://doi.org/10.1016/j.pocean.2023.102981

Brakstad, A., Våge, K., Håvik, L., & Moore, G. W. K. (2019). Water mass transformation in the Greenland Sea during the period 1986–2016. *Journal of Physical Oceanography*, *49*(1), 121–140. https://doi.org/10.1175/jpo-d-17-0273.1

Chatterjee, S., Raj, R. P., Bertino, L., Skagseth, Ø., Ravichandran, M., & Johannessen, O. M. (2018). Role of Greenland Sea Gyre circulation on Atlantic water temperature variability in the Fram Strait. *Geophysical Research Letters*, *45*(16), 8399–8406. https://doi.org/10.1029/2018gl079174

Comiso, J. C., Wadhams, P., Pedersen, L. T., & Gersten, R. A. (2001). Seasonal and interannual variability of the Odden ice tongue and a study of environmental effects. *Journal of Geophysical Research*, *106*(C5), 9093–9116. https://doi.org/10.1029/2000jc000204

Dickson, R., Lazier, J., Meincke, J., Rhines, P., & Swift, J. (1996). Long-term coordinated changes in the convective activity of the North Atlantic. *Progress in Oceanography*, *38*(3), 241–295. https://doi.org/10.1016/s0079-6611(97)00002-5

Fogelqvist, E., Blindheim, J., Tanhua, T., Østerhus, S., Buch, E., & Rey, F. (2003). Greenland–Scotland overflow studied by hydro-chemical multivariate analysis. *Deep Sea Research Part I: Oceanographic Research Papers*, *50*(1), 73–102. https://doi.org/10.1016/s0967-0637(02)00131-0

Germe, A., Houssais, M. N., Herbaut, C., & Cassou, C. (2011). Greenland Sea sea ice variability over 1979–2007 and its link to the surface atmosphere. *Journal of Geophysical Research*, *116*(C10), C10034. https://doi.org/10.1029/2011jc006960

Hansen, B., & Østerhus, S. (2000). North Atlantic–Nordic Seas exchanges. *Progress in oceanography*, *45*(2), 109–208. https://doi.org/10.1016/s0079-6611(99)00052-x

Hawker, E. J. (2005). *The Nordic Seas circulation and exchanges* (Doctoral dissertation). University of Southampton.

Hersbach, H., Bell, B., Berrisford, P., Biavati, G., Horányi, A., Muñoz Sabater, J., et al. (2023). ERA5 hourly data on pressure levels from 1940 to present [Dataset]. Copernicus Climate Change Service (C3S) Climate Data Store. https://doi.org/10.24381/cds.bd0915c6

Hersbach, H., Bell, B., Berrisford, P., Hirahara, S., Horányi, A., Muñoz-Sabater, J., et al. (2020). The ERA5 global reanalysis. *Quarterly Journal of the Royal Meteorological Society*, *146*(730), 1999–2049. https://doi.org/10.1002/qj.3803

Isachsen, P. E., Mauritzen, C., & Svendsen, H. (2007). Dense water formation in the Nordic Seas diagnosed from sea surface buoyancy fluxes. *Deep Sea Research Part I: Oceanographic Research Papers*, *54*(1), 22–41. https://doi.org/10.1016/j.dsr.2006.09.008

Jakobsen, P. K., Ribergaard, M. H., Quadfasel, D., Schmith, T., & Hughes, C. W. (2003). Near-surface circulation in the northern North Atlantic as inferred from Lagrangian drifters: Variability from the mesoscale to interannual. *Journal of Geophysical Research*, *108*(C8), 3251. https://doi.org/10.1029/2002jc001554

Kasajima, Y., & Johannessen, T. (2009). Role of cabbeling in water densification in the Greenland Basin. *Ocean Science*, *5*(3), 247–257. https://doi.org/10.5194/os-5-247-2009

Khosravi, N., Wang, Q., Koldunov, N., Hinrichs, C., Semmler, T., Danilov, S., & Jung, T. (2022). The Arctic Ocean in CMIP6 models: Biases and projected changes in temperature and salinity. *Earth's Future*, *10*(2), e2021EF002282. https://doi.org/10.1029/2021ef002282

Koenig, Z., Kalhagen, K., Kolås, E., Fer, I., Nilsen, F., & Cottier, F. (2022). Atlantic water properties, transport and heat loss from mooring observations north of Svalbard. *Journal of Geophysical Research: Oceans*, *127*(8), e2022JC018568. https://doi.org/10.1029/2022jc018568

Lauvset, S. K., Brakstad, A., Våge, K., Olsen, A., Jeansson, E., & Mork, K. A. (2018). Continued warming, salinification and oxygenation of the Greenland Sea gyre. *Tellus A: Dynamic Meteorology and Oceanography*, *70*(1), 1–9. https://doi.org/10.1080/16000870.2018.1476434

Legutke, S. (1991). A numerical investigation of the circulation in the Greenland and Norwegian Seas. *Journal of physical oceanography*, *21*(1), 118–148. https://doi.org/10.1175/1520-0485(1991)021<0118:aniotc>2.0.co;2

Lilly, J. M., & Rhines, P. B. (2002). Coherent eddies in the Labrador Sea observed from a mooring. *Journal of Physical Oceanography*, *32*(2), 585–598. https://doi.org/10.1175/1520-0485(2002)032<0585:ceitls>2.0.co;2

Lique, C., Johnson, H. L., Plancherel, Y., & Flanders, R. (2015). Ocean change around Greenland under a warming climate. *Climate Dynamics*, *45*(5), 1235–1252. https://doi.org/10.1007/s00382-014-2373-4

Lique, C., & Thomas, M. D. (2018). Latitudinal shift of the Atlantic Meridional Overturning Circulation source regions under a warming climate. *Nature Climate Change*, *8*(11), 1013–1020. https://doi.org/10.1038/s41558-018-0316-5

Mork, K. A., Drinkwater, K. F., Jónsson, S., Valdimarsson, H., & Ostrowski, M. (2014). Water mass exchanges between the Norwegian and Iceland seas over the Jan Mayen Ridge using in-situ current measurements. *Journal of Marine Systems*, *139*, 227–240. https://doi.org/10.1016/j.jmarsys.2014.06.008

Nurser, A. J. G., & Bacon, S. (2014). The Rossby radius in the Arctic Ocean. *Ocean Science*, *10*(6), 967–975. https://doi.org/10.5194/os-10-967-2014

Østerhus, S., & Gammelsrød, T. (1999). The abyss of the Nordic Seas is warming. *Journal of Climate*, *12*(11), 3297–3304. https://doi.org/10.1175/1520-0442(1999)012<3297:taotns>2.0.co;2

Petit, T., Lozier, M. S., Josey, S. A., & Cunningham, S. A. (2020). Atlantic deep water formation occurs primarily in the Iceland Basin and Irminger Sea by local buoyancy forcing. *Geophysical Research Letters*, *47*(22), e2020GL091028. https://doi.org/10.1029/2020gl091028

Segtnan, O. H., Furevik, T., & Jenkins, A. D. (2011). Heat and freshwater budgets of the Nordic Seas computed from atmospheric reanalysis and ocean observations. *Journal of Geophysical Research*, *116*(C11). https://doi.org/10.1029/2011jc006939

Shao, Q., Zhao, J., Drinkwater, K. F., Wang, X., & Cao, Y. (2019). Internal overflow in the Nordic Seas and the cold reservoir in the northern Norwegian Basin. *Deep Sea Research Part I: Oceanographic Research Papers*, *148*, 67–79. https://doi.org/10.1016/j.dsr.2019.04.012

Somavilla, R., Schauer, U., & Budéus, G. (2013). Increasing amount of Arctic Ocean deep waters in the Greenland Sea. *Geophysical Research Letters*, *40*(16), 4361–4366. https://doi.org/10.1002/grl.50775

Spall, M. A. (2010). Dynamics of downwelling in an eddy-resolving convective basin. *Journal of Physical Oceanography*, *40*(10), 2341–2347. https://doi.org/10.1175/2010jpo4465.1

Swift, J. H., & Aagaard, K. (1981). Seasonal transitions and water mass formation in the Iceland and Greenland seas. *Deep Sea Research Part A. Oceanographic Research Papers*, *28*(10), 1107–1129. https://doi.org/10.1016/0198-0149(81)90050-9

Swift, J. H., & Koltermann, K. P. (1988). The origin of Norwegian Sea deep water. *Journal of Geophysical Research*, *93*(C4), 3563–3569. https://doi.org/10.1029/jc093ic04p03563

Turrell, W. R., Slesser, G., Adams, R. D., Payne, R., & Gillibrand, P. A. (1999). Decadal variability in the composition of Faroe Shetland Channel bottom water. *Deep Sea Research Part I: Oceanographic Research Papers*, *46*(1), 1–25. https://doi.org/10.1016/s0967-0637(98)00067-3

Wadhams, P. (1981). The ice cover in the Greenland and Norwegian Seas. *Reviews of geophysics*, *19*(3), 345–393. https://doi.org/10.1029/rg019i003p00345

Wadhams, P., Comiso, J. C., Prussen, E., Wells, S., Brandon, M., Aldworth, E., et al. (1996). The development of the Odden ice tongue in the Greenland Sea during winter 1993 from remote sensing and field observations. *Journal of Geophysical Research*, *101*(C8), 18213–18235. https://doi.org/10.1029/96jc01440

Wang, X., Zhao, J., Hattermann, T., Lin, L., & Chen, P. (2021). Transports and accumulations of Greenland Sea intermediate waters in the Norwegian Sea. *Journal of Geophysical Research: Oceans*, *126*(4), e2020JC016582. https://doi.org/10.1029/2020jc016582